2015 Tenth International Conference on Ecological Vehicles and Renewable Energies (EVER)

Simplified model of eddy current brakes and its use for optimization

Christoph Holtmann
Institute of
Vehicle Concepts
German Aerospace Center
70569 Stuttgart, Germany
Email: christoph.holtmann@dlr.de

Frank Rinderknecht
Institute of
Vehicle Concepts
German Aerospace Center
70569 Stuttgart, Germany
Email: frank.rinderknecht@dlr.de

Horst E. Friedrich
Institute of
Vehicle Concepts
German Aerospace Center
70569 Stuttgart, Germany
Email: horst.friedrich@dlr.de

***Abstract*—The electrification of vehicles makes it possible to think about new concepts to substitute conventional technologies. For example in an electrical drive train, with a traction motor for each wheel mechanical friction brakes can be replaced by eddy current brakes. In this work a method for optimizing the torque density of eddy current brakes is presented. For a fast optimization process the model of the eddy current brake is split up in two levels of detail. In the first level a global model including a simplified eddy current model and a lumped parameter magnetic circuit to calculate the primary magnetic flux will be described. The second level includes a detailed eddy current model and will be described in further works. The simplified eddy current model include fitting parameters which allow to fit the torque curves to the ones of the detailed eddy current model. As a result, the method allows to optimize the entire system represented by the global model in a very fast way. The development of the global model, its verification and the method for optimizing the entire system represented by the global model is shown.**

I. Introduction

The most important parameters of eddy current brakes are their torque density and their torque characteristics. The analysis of the torque characteristics is only possible with simplified analytical models or FEM models. In [4] the torque characteristics of an eddy current brake with different copper layer thicknesses were calculated by using FEM analysis. The results were fitted with a characteristic function to analyse the braking performance during vehicle-dynamic simulations. In this work a model based fitting function is used to analyse the braking performance instead of a parameter-based fitting function (see equation (1) in [4]). The model based fitting function is a simple impedance model as in [1]. For a fast optimization process the analysis of the eddy current brake is split up in two models.

The first one, global model, describes the behaviour of the eddy current brake. The second one (detailed model) models the behaviour of the eddy currents in the eddy current area due to the air gap and the groove slot. The detailed model will be discussed in future works. To analyse the torque density of the entire eddy current brake the mass and volume of the magnetic excitation circuit has to be considered. Therefore the global model consists of a lumped parameter magnetic circuit and a simplified eddy current model. The connection between the global model and the detailed model is done by fitting the torque curves of the detailed model with the simplified eddy current model. In this work the development of the global model is described and its verification and the use of the optimization process is shown.

A. Characteristic quantities

The goal of the optimization is to find the geometric parameters of the eddy current brake (ECB) which result in a maximum torque density. Unlike electrical machines; which have a constant torque up to the nominal speed, the torque of ECBs increases up to a critical speed where the torque is at its maximum. At speeds higher than the critical speed the torque decreases. Figure I.1 shows qualitatively the torque curve of an ECB with its characteristic values. It can be seen that the torque density of ECBs can be defined in many ways. In past

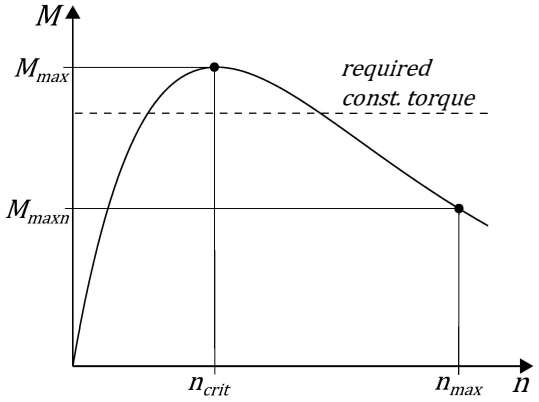

Fig. I.1: characteristic torque curve of an ECB

works the peak torque M_{max} and the critical speed n_{crit} were analysed. With the volume of an ECB V_{ecb} the peak torque density is

$$G_{max} = \frac{M_{max}}{V_{ecb}}. \quad (1)$$

For many applications the peak torque is not the most important factor. When a constant torque is required over the operation range, as illustrated in figure I.1, the torque density should be defined as the product of the middle torque density

978-1-4673-6785-1/15/$31.00 ø 2015 European Union

and the ratio of the middle torque density and the peak torque density. The middle torque density

$$G_m = \frac{1}{n_{max} V_{ecb}} \int_{n=0}^{n=n_{max}} M(n) \mathrm{d}n \tag{2}$$

could be identical for a flat torque curve and a torque curve with a high peak torque. When a constant torque is required and the torque curve has a high peak torque, the torque potential is not fully used. To design an ECB with a high torque in a wide operation range, the middle weighted torque density G_{mw} has to be maximized. G_{mw} is defined as

$$G_{mw} = \frac{1}{n_{max} V_{ecb}} \frac{1}{M_{max}} \left[\int_{n=0}^{n=n_{max}} M(n) \mathrm{d}n \right]^2 . \tag{3}$$

B. Eddy current model

The eddy current model used in this work consists of a conducting plate moving with the velocity v_m through an inhomogeneous primary magnetic field, represented with the magnitude $\triangle B = B^+ - B^-$ of the air gap flux density. The eddy currents are approximated in a single eddy current path with the resistances R_1, R_2 and R_3 as shown in I.2(a).

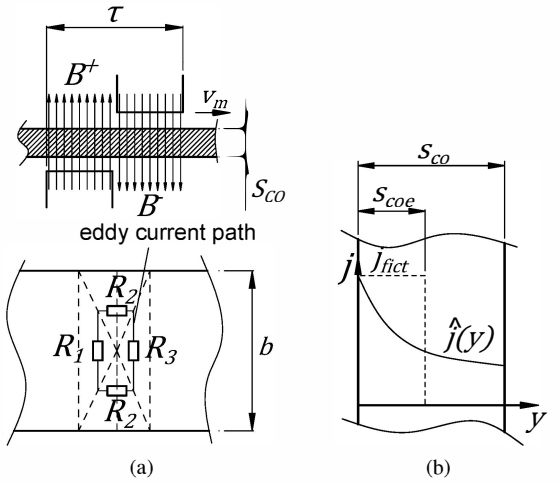

Fig. I.2: Model of a conducting plate moving with the velocity v_m through an inhomogeneous primary magnetic field while approximating the eddy currents in one eddy current path (a). Model for the effective thickness of the eddy current path (b).

During the movement with the middle velocity v_m, the induced voltage u_i in the eddy current path will be calculated by using Faraday's law of induction.

$$u_i = \oint_S \vec{v} \times \vec{B} \mathrm{d}S = (B^+ - B^-) 0.5 b v_m \tag{4}$$

is the formula for a voltage induction path length of $0.5b$. This length is also used to calculate the resistances R_1 and R_3 of the eddy current path.

$$R_1 = R_3 = c_R \frac{2b}{\sigma S_{COe} \tau} \tag{5}$$

$$R_2 = c_R \frac{\tau}{\sigma 2 b s_{COe}} \tag{6}$$

The total resistance of one eddy current path is

$$R = 2 c_R (R_1 + R_2). \tag{7}$$

The resistance factor c_R is used in equation (7) because the eddy currents are approximated only in one eddy current stream. The resistance factor is one of the fitting parameters to connect the detailed model with the simplified eddy current model.

To approximate the field repression the resistances are calculated with the effective thickness of the eddy current cross section s_{coe}. s_{ceo} is the thickness related to a fictive current I_{fict} in the homogeneous eddy current path. This fictive current is approximated by integrating the current density in a conducting half space on which a pulsating magnetic field is applied. The boundaries of the integration are the surfaces $y = 0$ and $y = s_{co}$ as shown in figure 9 (b).

$$I_{fict} = \int_{y=0}^{s_{CO}} \hat{i}(y) \mathrm{d}y = \hat{i}_{fict} s_{COe} \quad with \quad \hat{i}(y) = \hat{i}_s e^{\frac{y}{\delta}} . \tag{8}$$

This results in the effective thickness of the eddy current area

$$s_{coe} = \delta \left(1 - e^{-\frac{s_{co}}{\delta}} \right), \tag{9}$$

where δ is the penetration depth with the relative permeability μ_{rco} and the conductivity σ of the eddy current material.

$$\delta = \sqrt{\frac{\tau}{\pi v_m \mu_0 \mu_{rco} \sigma}} \tag{10}$$

In this context the relative permeability μ_{rco} is just a fitting parameter because the eddy current material has a non linear behaviour and is inhomogeneous in space.

As in equation 1 in [1] an inductance L is applied into the eddy current path, because the eddy currents are approximated only in one current stream. It is assumed that the inductance first of all is a result of the magnetic resistance of the air gap.

$$L = \frac{1}{R_{m\delta}} = \frac{\mu_0 c_L \tau b}{8 s} \tag{11}$$

Because the eddy currents are inhomogeneous the inductance factor c_L is used in equation 11 as a fitting parameter. The inductance results in an reactance

$$X = L\omega = L 2\pi \frac{v_m}{\tau}. \tag{12}$$

Due to the impedance $\underline{Z} = R + iX$ and the induced voltage, the current in the eddy current path is

$$I = \frac{u_i}{|\underline{Z}|} = \frac{u_i}{\sqrt{R^2 + X^2}}. \tag{13}$$

Equation (5) in [1] is quite similar to the equation above but the resistances are calculated differently. The model of [1] does not include the effect of the field repression represented by the effective thickness of the eddy current path as described in equation (9).

Due to the total power dissipation of the ECB $P = I^2 R N_{ecp}$ and the conservation of energy, the drag force of an eddy current brake can be approximated with

$$F = \frac{P}{v_m} = \frac{\triangle B^2 b^2 v_m}{4(R^2 + X^2)} R N_{ecp}, \tag{14}$$

where N_{ecp} is the number of eddy current paths.

The eddy current model is verified by using the results from FEM analysis and measurements of other publications [2] [3] [4]. The model should be independent of the magnitude of the ECB therefore papers with different sizes of eddy current brakes were chosen for the verification. The smallest was the ECB investigated in [2] and the biggest was investigated in [4]. To verify the ECB model equation (14) the torque or force curves from [2], [3] and [4] are fitted by using the least square method with the resistance factor c_R, the inductance factor c_L and the relative permeability μ_r as fitting parameters. Because the primary air gap flux density $\triangle B$ is not explicitly given in [2], [3] and [4] the magnitude of the air gap flux density is also used as a fitting parameter. The torque curves from [2], [3] and [4] are transformed to force speed curves with the middle active radius r_m using

$$F = M/r_m \quad and \quad v_m = r_m\omega = r_m 2\pi n. \tag{15}$$

This allows the comparison of the radial-flux-ECB in [3] with the axial-flux-ECBs in [2] and [4]. The geometric data from [3] is extracted from figure 1 and 2 in patent [9] while the rotor diameter is given in figure 3 in [9]. From [3] the torque curve given in [9] with no copper layer is used. It must be pointed out that the velocity in figure 1 in [4] is the train speed. The radius of the wheel is $0.460m$ while the middle active radius is $r_m = 0.2625m$. The parameters utilized for the verification from [2], [3] [9] and [4] are shown in table I.1.

Figure I.3 shows qualitatively the result of the verification. Due to the fitted torque curves, the quantitative results are

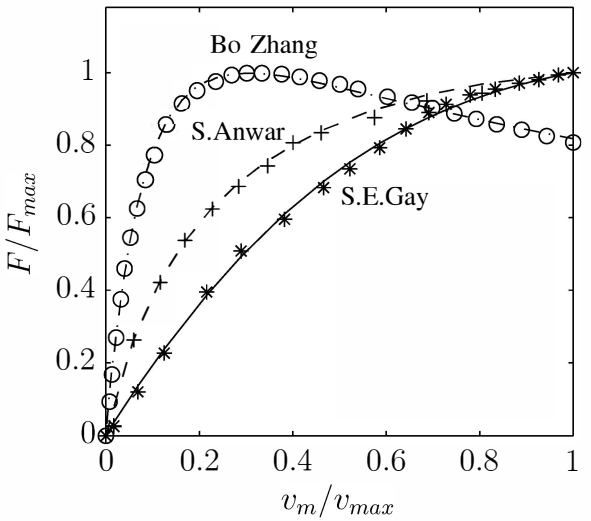

Fig. I.3: Braking force vs. speed of different ECB, data from [3, S. Anwar],[4, Bo Zhang] and [2, S.E.Gay] (markers) and model based fitted curves (lines) $v_{max} = 9.68m/s$ $F_{max} = 44.47N$ (S.E.Gay), $v_{max} = 22.26m/s$, $F_{max} = 6145N$ (S.Anwar), $v_{max} = 55.42m/s$, $F_{max} = 16086N$ (Bo Zhang).

shown in table I.2. The maximum error related to the maximum torque

$$e = \frac{|F_{fit} - F_{ref}|}{F_{max,ref}} \tag{16}$$

from every fitted torque curve is less then 4 %.

TABLE I.1: Parameter of the ECBs from [2], [3] and [4] needed for the verification, the conductivity of the ECB from [3] \[9] is not explicitly given, a conductivity of carbon steel is used[(1)]

Parameter	Bez.	Gay [2]	S. Anwar [3]	Bo Zhang [4]
middel active radius	$r_m[m]$	0.0508	0.1225	0.2625
width eddy current-element	$b[m]$	0.0254	0.095	0.232
thickness of eddy current element	$s_{C\bullet}[m]$	0.00317	0.0086	0.0325
width of one pole pair	$\tau[m]$	0.04	0.064	0.412
number of eddy current pathes	$N_{E\bullet}[1]$	16	24	8
conductivity reference [2] [3] [4]	$\sigma[\Omega^{-1}m^{-1}]$	17e6	4.5e6[(1)]	4.55e6

TABLE I.2: Fitted parameter of the ECBs from [3], [2] and [4]

Parameter	Bez.	Gay [2]	S. Anwar [3]	Bo Zhang [4]
amplitude air gap flux density	$\triangle B_{fit}[T]$	0.935	2.48	1.62
resistance factor	c_{R}	0.857	1.1	2.02
inductance factor	c_L	0.965	0.2	0.21
relative permeability (fit)	μ_{rfit}	7.5	29.2	8.2
maximum error	e_{max}	0.022	0.032	0.023

To evaluate experimental results only the resistance factor c_R, the inductance factor c_L and the relative permeability μ_r will be used because the primary magnetic field can be measured. The primary magnetic field is not explicitly given in the publications of [2],[3] and [4]. In [4] the torque characteristics for different air gap thicknesses was analysed. In this work a 2-D-FEM model of the ECB from [4] is built up to analyse the air-gap flux density. The maximum flux density is used to fit the curves given in figure 10 in [4] while using c_R,

TABLE I.3: Fitted parameter of the ECB from [4] with the variation of the air gap thickness.

$\delta[mm]$	3	5	8	12
$\triangle B[T]$	1.68	1.62	1.54	1.46
c_{R}	1.99	2.02	2.02	2.576
c_L	0.168	0.194	0.223	0.242
μ_{rfit}	5.45	8.2	11.58	7.6
e_{max}	0.023	0.03	0.033	0.023

c_L and μ_r as fitting parameters. Figure I.9 shows the results of the 2-D-FEM calculation of the air gap flux density on the rotor surface. The maximum flux density due to the different air gap thicknesses and the fitting results of c_R and c_L are given in table I.3.

It can be seen that the correlation between the fitting parameters (resistance factor, the inductance factor and the relative permeability) and the air gap, cannot be described in a simple way. This correlation will be more precisely analysed with the detailed model in future papers.

To test the optimization process of the global model developed in this work, the resistance factor c_R, the inductance factor c_L and the relative permeability μ_r are set to one.

C. Dimensionless parameters and geometry

The optimization should be independent of the ECB's magnitude and the analysis of the torque density is done with dimensionless variables and parameters. The pattern of eddy currents and therefore the torque characteristics first of all depends on the magnetic Reynolds Number as shown in [5]. The middle velocity v_m of the moving eddy current material, the width of one pole pair τ and the conductivity are the characteristic quantities.

$$Rm_\tau = v_m \tau \sigma \mu_0 \tag{17}$$

For the eddy current brake optimized in this work, as shown in figure I.4, the velocity is $v_m = r_o(1+r_i^*)\omega/2$ and the width of one pole pair is $\tau = r_o\pi(1+r_i^*)/N_{pp}$. This results in the magnetic Reynold Number

$$Rm_\tau = \frac{r_o^2}{2N_{pp}}(1+r_i^*)^2\omega\sigma\mu_0 \tag{18}$$

with the outer radius r_o as characteristic quantity.

One of the most limiting parameter of ECBs is the current density of the excitation coils $i_{cmax} = j_0$. In the case of a linear magnetisation curve the primary magnetic field is proportional to the excitation current $I_{cmax} \sim i_{cmax} r_o^2$ due to the magnetic resistance of the magnetic excitation circuit $R_{mep} \sim 1/(\mu_0 r_o)$. This results in the reference flux density

$$B_0 = i_{cmax}\mu_0 r_o. \tag{19}$$

Magnetic resistances are related to $R_{m0} = 1/(\mu_0 r_0)$

$$R_m^* = \frac{R_m}{R_{m0}} = R_m \frac{\mu_0 r_0}{\delta^*} \tag{20}$$

and magnetic strain to $V_0 = r_0^2 i_0$. Electrical resistances are related to $R_0 = 1/(\sigma r_o)$.

The geometry of the ECB, which is optimized in this work, is shown in figure I.4. For the optimization process geometric parameters are defined which can only reach values from zero to one. All geometric parameters are directly or indirectly related to the outer radius r_o and are always related to its possible maximum except of the aspect ratio λ and the air gap δ^*. The definitions of the geometric parameters are given in table I.4.

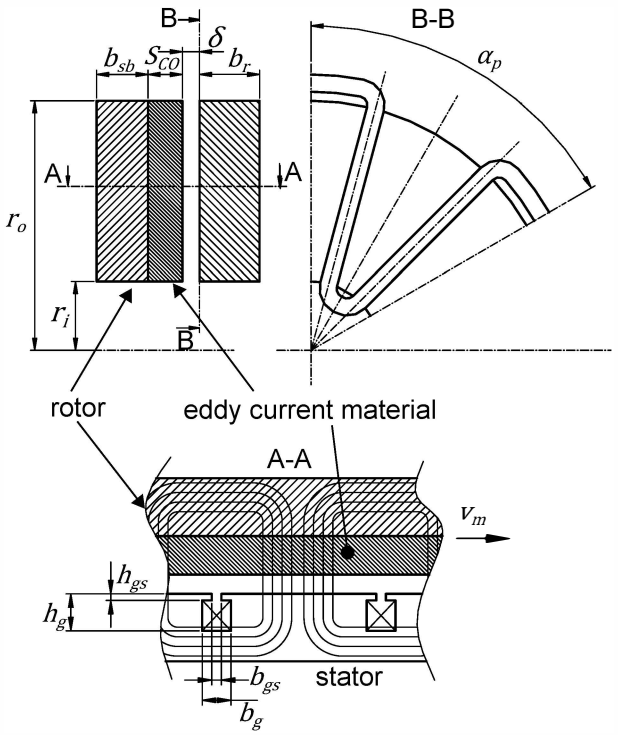

Fig. I.4: geometry of the ECB optimized in this work

TABLE I.4: Definition of geometric parameters

ratio	def.
aspect ratio	$\lambda = \frac{b}{2r_o}$
inner radius to outer radius	$r_i^* = \frac{r_i}{r_o}$
air gap to outer radius	$\delta^* = \frac{\delta}{r_\bullet}$
width rotor to max. width Rotor	$b_r^* = \frac{b_r}{r_\bullet 2\lambda - \delta} = \frac{b_r}{r_\bullet(2\lambda - \delta^*)}$
width eddy current element to max. width eddy current element	$S_{C\bullet}^* = \frac{S_{C\bullet}}{r_\bullet 2\lambda - \delta - b_r} = \frac{S_{C\bullet}}{r_\bullet(2\lambda - \delta^*)(1 - b_r^*)}$
width groove to max. width groove	$b_g^* = \frac{b_g}{b_{gmax}} = \frac{b_g}{2r_o r_i^* \sin\left(\frac{\pi}{2N_{pp}}\right)}$
hight groove with groove slot to width rotor	$h_g^* = \frac{h_g}{b_r} = \frac{h_g}{r_o b_r^*(2\lambda - \delta^*)}$
width groove slot to width groove	$b_{gs}^* = \frac{b_{gs}}{b_g} = \frac{b_{gs}}{r_o 2b_g^* r_i^* \sin\left(\frac{\pi}{2N_{pp}}\right)}$
higth groove slot to hight groove with groove slot	$h_{g_s}^* = \frac{h_{g_s}}{h_g} = \frac{h_{g_s}}{r_\bullet h_g^* b_r^*(2\lambda - \delta^*)}$

The application of the dimensionless parameters to the equations of the eddy current model gives for equation (7)

$$R^* = \frac{c_R}{s_{ceo}^*}\left(\frac{4(1-r_i^*)N_{pp}}{\pi(1+r_i^*)} + \frac{\pi(1+r_i^*)}{N_{pp}(1-r_i^*)}\right) \tag{21}$$

where s^*_{coe} (see equation 9) is

$$s^*_{coe} = \delta^*_{ec}\left(1 - e^{-\frac{s^*_{coe}(2\lambda - \delta^*)(1 - b^*_r)}{\delta^*_{ec}}}\right) \tag{22}$$

with

$$\delta^*_{ec} = \sqrt{\frac{\pi(1 + r^*_i)}{N^2_{pp} Rm_\tau \mu_{rco}}} \tag{23}$$

Equation (12) using equation (11) results in

$$X^* = \frac{c_L}{\delta^*} \frac{N_{pp}(1 - r^*_i)}{4(1 + r^*_i)} Rm_\tau. \tag{24}$$

The induced voltage can be written in dimensionless form as

$$u^*_i = \triangle B^*_\delta \frac{N_{pp}(1 - r^*_i)}{2\pi(1 + r^*_i)} Rm_\tau. \tag{25}$$

With $P = u^2_i R/Z^2$ and $M = P/\omega$ the torque in dimensionless form is

$$M^* = \frac{\triangle B^{*2}_\delta (1 - r^*_i)^2 N^2_{pp}}{4\pi(X^{*2} + R^{*2})} R^* Rm_\tau. \tag{26}$$

The dimensionless form of the torque density is

$$G^* = \frac{\triangle B^{*2}_\delta (1 - r^*_i)^2 N^2_{pp}}{8\lambda\pi^2(X^{*2} + R^{*2})} R^* Rm_\tau \tag{27}$$

D. Lumped parameter magnetic circuit

To approximate the air gap flux density B_δ a lumped parameter magnetic circuit shown in figure I.5 is modelled. The current in the excitation coils causes the magnetic strain V_m. In dimensionless form the magnetic strain is

$$V^*_m = 2b^*_g r^*_i \sin\left(\frac{\pi}{2N_{pp}}\right) h^*_g b^*_r (2\lambda - \delta_s)(1 - h^*_{gs}). \tag{28}$$

.

The magnetic resistances R_{m2} and R_{m3} are calculated with the respective length of the flux path l_i, its cross section A_i and its permeability $\mu_i = \mu_0 \mu_{ri}$

$$R_i = \frac{l_i}{\mu_0 \mu_{ri} A_i}.$$

The magnetic resistances R_{m1}, R_{m4} and R_{m5} are the sum of the magnetic resistances of flux paths in radial and axial direction. Given from [7] the magnetic resistances R_{m0} and R_{m6} are

$$R_{m1} = R_{m6} = \frac{1}{\mu_0 0.26t} \quad with \quad t = r_o(1 - r^*_i) \tag{29}$$

The magnetic resistances are given in dimensionless form in table I.7. The linear equation system including 5 mesh and 4 node equations is solved iteratively using the magnetisation curve of steel 1008 for the resistances R_{m1}, R_{m2} and R_{m5}. The relative permeability is interpolated as a function of the flux density while using the flux density in the respective cross section. For interpolating the real flux density

$$B = B_0 B^* = j_{cmax} \mu_0 r_o B^* \tag{30}$$

is needed. Hence the optimal design parameters in table I.4 depend on the main dimension, the outer radius r_o.

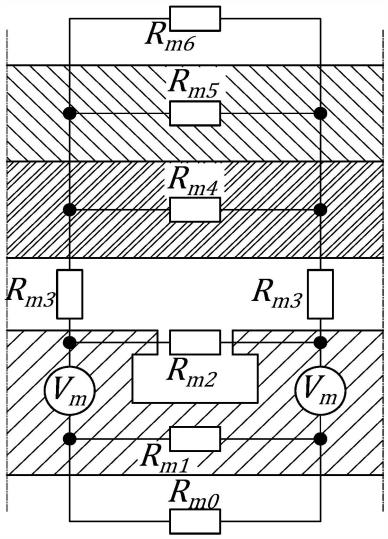

Fig. I.5: Lumped parameter magnetic circuit

The lumped parameter magnetic circuit is verified with a 2D-FEM-analysis using the parameters in table I.5 with $b^*_r = 0.7$ and $b^*_r = 0.8$.

TABLE I.5: Parameters that are used to verify the lumped parameter magnetic circuit with a 2-D-FEM-calculation

$r_\bullet[m]$	λ	$\delta^*[1]$	$N_{ec\bullet}[1]$	$r^*_i[1]$
0.15	0.2	0.01	4	0.5
$s^*_{c\bullet}[1]$	$b^*_g[1]$	$b^*_{gs}[1]$	$h^*_g[1]$	$h^*_{gs}[1]$
0.5	0.5	0.6	0.2	1

Figure I.6 shows the flux density magnitude in areas with the highest saturation. The discrepancy between the analytical and FEM solution in this areas is less then 10%.

To examine the connection between the eddy current model and the lumped parameter magnetic circuit the torque curves for different excitation currents are calculated using the geometric parameters given in table I.6. The calculation is done by using the simplified eddy current model. This includes the air gap flux density that is calculated with the lumped parameter magnetic circuit. The resulting torque curves can be compared with the torque curves in figure 8 in [4], because the same geometric parameters are used. For the calculation the fitted parameters for an air gap of 5mm and an excitation current of $88A$ are used ($c_R = 2.02$, $c_L = 0.194$ and $\mu_r = 8.2$, table I.3).

Figure I.7 shows the torque curves calculated with the simplified eddy current model and the lumped parameter magnetic circuit (lines) and the torque curves as the result of a FEM-calculation of [4] for different excitation currents ($I = 52A; 76A; 100A; 124A$). It can be seen that the torque curves calculated with the global model for a excitation current of $I = 52A$, $I = 100A$ and $I = 124A$ do not fit very well to the curves of [4]. This is because the relative permeability in the eddy current area changes due to the not linear magnetisation curve.

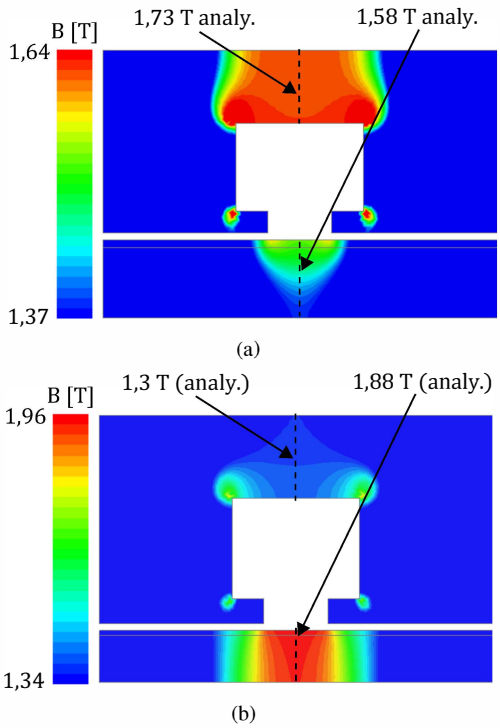

Fig. I.6: Magnitude of the flux density in areas of highest saturation of a 2D-FEM analyses (a) $b_r^* = 0.7$ (b) $b_r^* = 0.8$ using the parameters in table I.5

TABLE I.6: Parameters, extracted from [4], that are used to examine the connection between the simplified eddy current model and the lumped parameter magnetic circuit

$r_{\bullet}[m]$	$N_{ec\bullet}[1]$	$\tau_{\bullet\bullet}[m]$	$s_{c\bullet}[m]$	$\sigma[\Omega^{-1}m^{-1}]$	$\lambda[1]$	$\delta^*[1]$
0.375	8	0.412	0.0325	4.55e6	0.197	0.013
$r_i^*[1]$	$b_r^*[1]$	$s_{c\bullet}^*[1]$	$b_{\bullet}^*[1]$	$b_{\bullet s}^*[1]$	$h_{\bullet}^*[1]$	$h_{\bullet s}^*[1]$
0.4	0.745	1	0.7	0.18	0.64	0.21

E. Optimization method of the global model

An interval search method as described in [8] is used to determine the geometric parameters which result in a maximum torque density. The unknown function is calculated in an interval x_{left} x_{right} with two inner points as shown in figure I.10. If one inner point is the maximum value of the four points, the neighbour points of this point will be chosen as the next interval bounds. If the maximum value of the four points is located at the right bound, the next interval is between the point left to the maximum point and the point one step right of the maximum point. The same, in a mirrored way, will be done if the maximum value of the four points is located at the left bound. The process is repeated until the difference of one location where the maximum occurs $x_{max}(i)$ and the location of the maximum one step before $x_{max}(i-1)$ is

$$\triangle x = |x_{max}(i) - x_{max}(i-1)| < \triangle x_{max}.$$

This method works because the maximum of the torque density is a global maximum for each parameter. This method is used to optimize each parameter while using a multidimensional

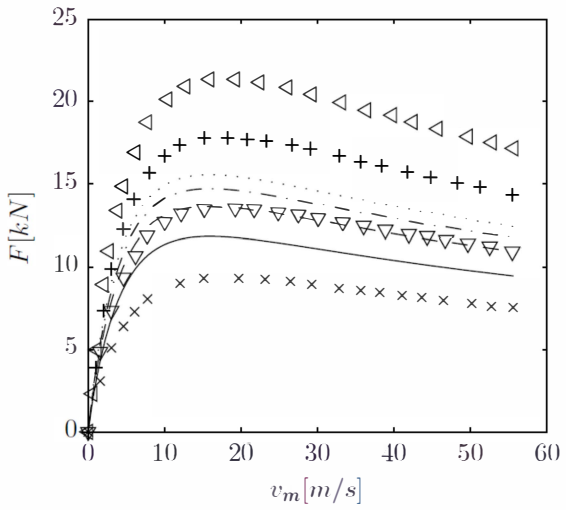

Fig. I.7: Braking force vs. speed for different excitation currents, data from [4] (markers) and torque curves based on the global model (lines) $I = 52A$ crosses and solid line, $I = 76A$ down triangles and dashed line, $I = 100A$ + and dash dot line and $I = 124A$ left triangles and doted line.

TABLE I.7: dimensionless magnetic resistances

region	equation
air at rotor	$R_{m0}^* = \frac{2}{(1-r_i^*)N_p}$
rotor	$R_{m1}^* = \frac{1}{\mu_{r11}} \frac{\frac{\pi}{2N_{\bullet\bullet}}(1+r_i^*) + b_g^* r_i^* \sin\left(\frac{\pi}{2N_{\bullet\bullet}}\right)}{b_r^*(2\lambda-\delta^*)(1-h_{\bullet}^*)(1-r_i^*)} + \frac{1}{\mu_{r12}} \frac{b_r^*(2\lambda-\delta^*)(1+h_g^*)}{\frac{\pi}{N_{\bullet\bullet}}(1-r_i^{*2}) - (r_i^*-r_i^{*2}) b_g^* \sin\left(\frac{\pi}{N_{\bullet\bullet}}\right)}$
groove slot	$R_{m2}^* = \frac{b_{gs}^* b_g^* r_i^* \sin\left(\frac{\pi}{2N_{pp}}\right)}{\mu_{r2}\lambda b_r^* h_{gs}^* h_g^* (1-r_i^*)}$
air gap	$R_{m3}^* = \frac{\delta^*}{\frac{\pi}{2N_{\bullet\bullet}}(1-r_i^{*2}) - (r_i^*-r_i^{*2}) b_{gs} b_g^* \sin\left(\frac{\pi}{2N_{\bullet\bullet}}\right)}$
eddy current element	$R_{m4}^* = \frac{1}{\mu_{r4}} \left[\frac{S_{CO}^*(2\lambda-\delta^*)(1-b_r^*)}{\frac{\pi}{2N_{\bullet\bullet}}(1-r_i^{*2}) - (r_i^*-r_i^{*2}) b_{gs} b_g^* \sin\left(\frac{\pi}{2N_{\bullet\bullet}}\right)} + \frac{\frac{\pi}{2N_{\bullet\bullet}}(1+r_i^*) + b_{\bullet s}^* b_{\bullet}^* r_i^* \sin\left(\frac{\pi}{2N_{\bullet\bullet}}\right)}{S_{CO}^*(2\lambda-\delta^*)(1-b_r^*)(1-r_i^*)} \right]$
stator back	$R_{m5}^* = \frac{1}{\mu_{r51}} \frac{(2\lambda-\delta^*)(1-S_{C\bullet}^*(1-b_r^*)-b_r^*)}{\frac{\pi}{2N_{\bullet}p}(1-r_i^{*2}) - (r_i^*-r_i^{*2}) b_{gs} b_{\bullet}^* \sin\left(\frac{\pi}{2N_{\bullet\bullet}}\right)} + \frac{1}{r_{\bullet}\mu_{\bullet}\mu_{r52}} \frac{\frac{\pi}{2N_{\bullet\bullet}}(1+r_i^*) + b_{gs}^* b_g^* r_i^* \sin\left(\frac{\pi}{N_{\bullet\bullet}}\right)}{(2\lambda-\delta^*)(1-S_{C\bullet}^*(1-b_r^*)-b_r^*)(1-r_i^*)} + \frac{1}{\mu_{r4}} \frac{S_{C\bullet}^*(2\lambda-\delta^*)(1-b_r^*)}{\frac{\pi}{2N_{\bullet\bullet}}(1-r_i^{*2}) - (r_i^*-r_i^{*2}) b_{gs} b_g^* \sin\left(\frac{\pi}{2N_{\bullet\bullet}}\right)}$

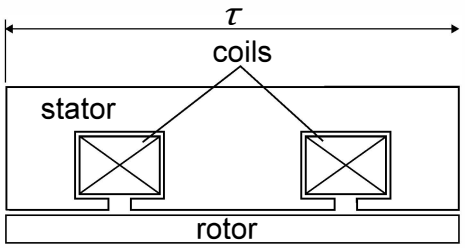

Fig. I.8: 2-D-FEM-Model to calculate the air gap flux density from the ECB of [4]

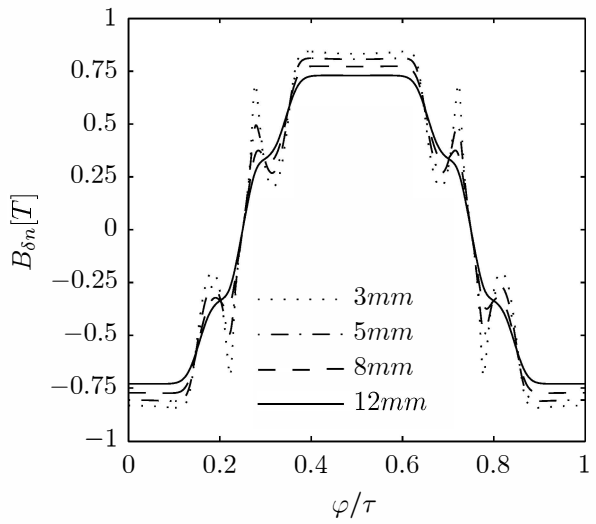

Fig. I.9: Calculated air gap flux density at the rotor surface at different air gap thicknesses using the geometry from the ECB of [4]

optimization method. The algorithm for optimising N parameters contains N nested loops as shown in figure I.11. The inner loop searches for the optimal parameter x_1 that results in a maximum torque density by calculating the global model while using the parameters that variate during the outer loops. Each parameter will be optimized using the optimal parameters that are found in the inner loops, except of the first. After the first optimal parameter in an inner loop is found during the parameter variation of a loop, this parameter is used as the start value of the interval search method of the inner loop for the next step of the loop. This decreases the convergence time of each inner loop during the interval search method.

The optimization of the dimensionless middle weighted torque density G^*_{mw} is done by using the constant parameters in table I.8,a maximum magnetic Reynolds number, corresponding with n_{max}, of $Rm_{max} = 1$ and a convergence criterion of $\triangle x_{max} = 0.02$. The width b^*_{gs} and the hight h^*_{gs} of the groove slot will be optimized with the detailed model. The optimization of five parameters took three hours using Matlab R2007b on a Intel(R) Core(TM)i7-3770 @ 3,4 GHz.

Figure I.12 shows the verification of the optimization method. It is done by the variation of each parameter while the others are at their optimum. It can be seen that the optimal geometric parameters are found with the optimization method

TABLE I.8: Constant parameters of the optimization process

$r_\bullet[m]$	$N_{\bullet\bullet}[1]$	$j_\bullet[Am^{-2}]$	$\sigma[\Omega^{-1}m^{-1}]$	δ^*	$b^*_{\bullet s}[1]$	$h^*_{\bullet s}[1]$
0.150	8	6e6	5e6	0.005	0.5	0.1

because all parameters result in the same torque density at their maximum represented with the horizontal dashed line.

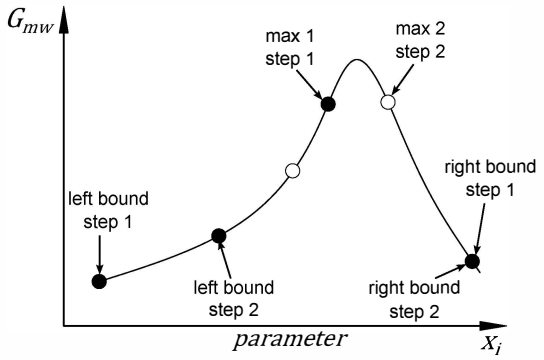

Fig. I.10: interval search method

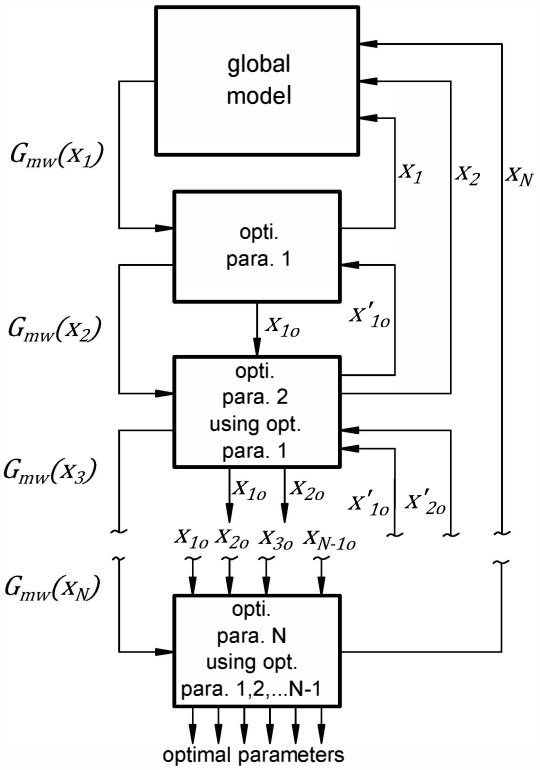

Fig. I.11: global optimization algorithm

II. Conclusion

In this work the development of a simplified eddy current model is shown. The connection between the detailed model and the simplified eddy current model including fitting parameters is done by fitting the torque curves of ECBs analysed in other works with the simplified eddy current model. The

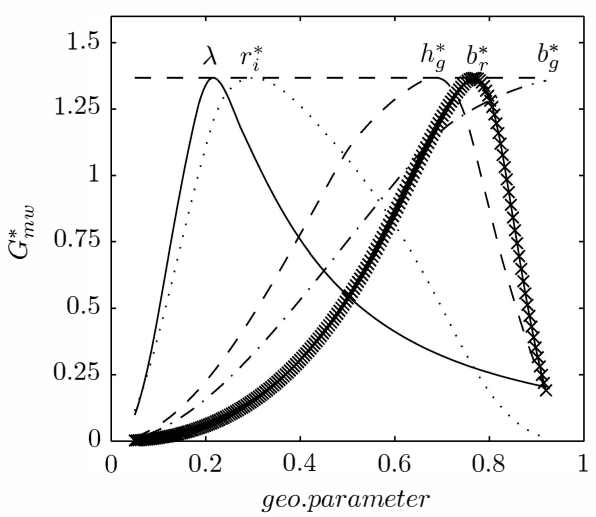

Fig. I.12: verification of the optimization method, the parameter for a respective line are signed up over the respective maximum

error of the fitting is less than 4 %. The relation between the geometries of the eddy current area and the pole tooth with the fitting parameters has to be analysed more precisely with experiments and the detailed model. This will be presented in future publications.

The lumped parameter magnetic circuit is verified with an error of less than 10% with a 2-D-FEM-model. Because the flux density is inserted with a square to the torque equation, the lumped parameter magnetic circuit has to be improved. Using the torque of different excitation currents, the connection between the lumped parameter magnetic circuit and the simplified eddy current model is examined by using the results of [4]. Because the material behaviour is not linear, the connection between the simplified eddy current model and the lumped parameter magnetic circuit has to be analysed by using the fitting parameters as a function of the primary magnetic flux. This will be done with the detailed model and experimental measurements. It is shown that the optimization method of the global model works with a accuracy of 2%. It has to be pointed out that the accuracy of the optimization of a real eddy current brake depends on the accuracy of the global model. The accuracy, as mentioned before, will be improved with the detailed eddy current model. Up to now there is no indication that the optimization method will work with a higher convergence time when the fitting parameters are more precisely analysed with the detailed model.

ACKNOWLEDGMENT

The authors would like to thank all colleagues and students working at the eddy current brake project.

REFERENCES

[1] Powell, E. F., and Gough, S. W. *Eddy current brakes.* Journal of Scientific Instruments 12.5 (1935): 161.

[2] Gay, S. E., and Ehsani, M. *Optimized design of an integrated eddy-current and friction brake for automotive applications*. Vehicle Power and Propulsion, IEEE Conference (2005): 290-294

[3] Anwar, S. and Stevenson, R. C. *Torque Characteristics Analyses for optimal design of a copper-layered eddy current brake.* International Journal of Automotive Technology (2011): 497-502

[4] Zhang, B., et al. *3-D nonlinear transient analysis and design of eddy current brake for high-speed trains.* International Journal of Applied Electromagnetics and Mechanics 40.3 (2012): 205-214.

[5] Guermond, J. L., J. Lorat, and C. Nore. "A new Finite Element Method for magneto-dynamical problems: two-dimensional results." European Journal of Mechanics-B/Fluids 22.6 (2003): 555-579.

[6] Barnes, Lee, et al. "An eddy current braking system." System Theory, 1993. Proceedings SSST'93., Twenty-Fifth Southeastern Symposium on. IEEE, 1993.

[7] Kallenbach, et al. "Elektromagnete". Vieweg+ Teubner Verlag, 2012. 125-187.

[8] Park, Gyung-Jin. Analytic methods for design practice. Germany: Springer, 2007.

[9] Li, Zhesheng, and Randy C. Stevenson. "Increased torque in retarder brake system through use of conductive layer." U.S. Patent No. 6,900,569. 31 May 2005.